International Journal of Bridge Engineering (IJBE), Vol. 8, No. 2, (2020), pp. 01-24

BEHAVIOR OF LINK SLAB BRIDGE GIRDERS WITH JOINTLESS DECK

Asmaa Mostafa[1], Laila Radwan[2], Ahmed Gadellah[2], Ahmed Elmanney[3]

[1,3] Misr University for Science and Technology, Egypt.
[2]Cairo University, Egypt.
e-mail: asmaa.mostafa@must.edu.eg, lradwan@yahoo.com,Atefgad111@gmail.com, asayed23@hotmail.com.

ABSTRACT: Link slabs represent a new technique to overcome the drawbacks of expansion joints. Despite the vital role of expansion joints in the relief of undesirable stresses in bridge structure, they can be considered a main source of its degradation. Link slabs are utilized over the piers developing jointless decks while adjacent bridge spans remain simply supported. This study focuses on the behavior of link slabs mounted on prestressed girder bridges instead of conventional expansion joints. A group of 3D models is built to simulate such bridge, while taking into consideration the effect of link slab length, configuration, material, and bridge's support condition on the generated straining actions in the link slab. Also, the effect of link slab on the main girder moment is tracked. It is found that straining actions in the mid-section of link slab decrease with the increase of the debonding zone length. Also, the presence of link slab in bridge with hinged-roller-roller-hinge support configuration leads to detrimental effects on both the link slab and the girder itself. Moreover, the conventional concrete material is not suitable, from stresses and serviceability points of view, for this type of slab especially if its thickness is small compared to the bridge's deck thickness. Engineered Cementitious Composite (ECC) can be used instead to withstand the generated stresses in the link slab.

KEYWORDS: Link Slab, Bridge, Expansion Joint, Girder, Model, Support, Engineered Cementitious Composite.

1 INTRODUCTION

Expansion joints role is to relieve the undesirable straining actions in bridge's structure, such as those related to thermal stresses, live load and long-term deformations [1]. These joints require continuous and elaborate maintenance process. The improper maintenance schedule and/or quality may lead to direct and indirect problems. The direct problems are related to the accumulation of debris in the joints which restrains deck's expansion. Also, water leakage through the joints induced corrosion problem in the bridge's different elements.

Moreover, the presence of the deteriorated expansion joints leads to severe increase in the propagated dynamic stresses in the adjacent structural elements [1, 2].

The indirect problems are related to traffic delays during the maintenance process, and to the repair costs of the vehicles passing the defected joints [2]. Therefore, the decrease or even the removal of the expansion joints will positively affect the economics of bridges [3-5].

To overcome the problems of expansion joints, continuous bridges were suggested. However, the required deck reinforcement was found to be excessive and the reinforcement details of the end diaphragm element make it difficult to execute in field [6]. Moreover, this type of sophisticated structures requires more advanced monitoring and maintenance programs [7].

Recently, the researchers developed the jointless decks system known as link slab which is a segment of the deck connecting the two adjacent simple-span girders. The total length of the link slab consists of the debonding and transition zones, and this length may reach up to 20% of the girder span based on the stiffness of the link slab. The link slab is totally disconnected from the girder at the mid zone, i.e. debonding zone. While, the transition zones are introduced at the edges of link slab to assure the continuity and stress transition between link slab and the rest of the bridge [4, 5, 8-20].

Several methods were proposed for analyzing the jointless deck systems [18-21]. Most of these methods depend on the finite element method. Early work considered simplified computational methods by modeling the girders and deck by two-noded isoparametric beam element and link slab by two-noded uniaxial spring-like element [18]. This procedure simplified the interaction between the girders and link slab while not considered the contact effect in the debonding zone or the bending stiffness of link slab.

In order to reduce stresses in link slab and consequently the cracks in its mid-zone, the concept of the debonded length between girder and deck was introduced [13]. Adjusted [9] 2D finite element models were built to model this zone and to study the effect of different support conditions on the induced stresses in link slab [19, 20].

It was found that these models failed in forecasting the behavior of the jointless decks [21].The difference between experimental results and model predictions referred to the bending stiffness contribution of link slab in addition to its axial stiffness. The experimental work conducted on two-span jointless bridge decks with steel and prestressed concrete girders with roller supports under link slab and hinged supports at edges of girders (HRRH) showed that the link slab was subjected to tension and bending [21], while, El-Safty's analysis predicted that the link slab was subject to compression only [3].

Other improvements on link slab modelling were elaborated in order to achieve a practical design methodology and concluded that support conditions represent an important role in the stress and strain interactions at the joint [3].

Moreover, the study of the influence of link slab on the performance of overall bridge showed that the induced stresses in the superstructure were more reasonable in case of partial continuity rather than full contact link slab [22].

Based on the results of the analysis, it was concluded that support conditions greatly affected on the link slabs behavior. RHHR support configuration led to imposing link slab to combined moment and axial force [23]. The authors suggested incorporating the additional moment and axial force produced from thermal gradient loads to the link slab design. A new method has been proposed for the analysis of link slabs that include the use of axial load with a moment in the interaction diagram, that's for particular support condition at link slab, it has been subjected to axial loads and flexural. [23].

The need to improve the understanding behavior of link slab by idealized models led to increasing the number of surveys, field investigations and structural system monitoring have been used to evaluate various performance criteria for the effectiveness of the link slab [24, 25].

The development of a large-width tensile crack on the top face of the link slab due to the utilization of conventional concrete was noticed. Though heavily steel reinforced link slab would have reduced the width of crack to the acceptable limits, but it would increase the stiffness of the link slabs. Moreover, if this crack is not correctly handled, this will cause degradation of the structure as these cracks, similarly to the expansion joints, would allow saltwater to contact the steel girder and rebar, causing corrosion problems [19, 21].

In order to overcome the cracks problem in link slab, innovative materials such as, Engineered Cementitious Composite (ECC) material and Fiber Reinforced Polymer (FRP) rebars were suggested to replace conventional concrete and steel rebars, respectively [19]. ECC is a unique type of High-Performance Fiber Reinforced Concrete (HPFRC) that offers significant potential for resolving the durability performance of reinforced and pre-stressed concrete structures [20-23]. The high strain hardening characteristic and multiple micro-cracking behaviors under tension and flexure while reducing the amount of the reinforcing fibers (less than 2% by volume) make it an ideal material for the link slab application. It is worth to mention that the tensile strain capacity of ECC is about 370 times that of traditional concrete [23, 24].

GFRP rebars are being applied increasingly in the construction industry, mostly due to their non-corrosive nature and high load bearing capacity. FRPs exhibit a linear- elastic load – deformation response and generally have lower elastic modulus than steel [19].

It is obvious that there is an indispensable need to study the performance of link slab, particularly, when fabricate with innovative materials. In this work, link slab performance is studied by means of a parametric study of partial depth of link slab with minimum reinforcement ratio and different varieties of conventional and innovative materials were studied. Moreover, other parameters were considered; link slab length, debonding zone length and support condition,

and its response was monitored under gravity and live loads. A recommendation of the best performance link slab configuration was delivered at the end of this work.

2 NUMERICAL MODEL

2.1 Verification model

The behavior of link slab, mounted on two simple span girder bridge, has been studied in lab. The strains, loads, crack growth, and deflections were monitored during the test. Full configuration of the test setup is shown in Figure 1. The testing load was applied at the mid-span of each girder. The point load was increased incrementally to 40% of the estimated ultimate capacity of the tested beam. Various support condition configurations were also examined. The support configurations from left to right were HRRH, RHRH and RHHR. (H stands for hinge support and R stands for roller support). [13]

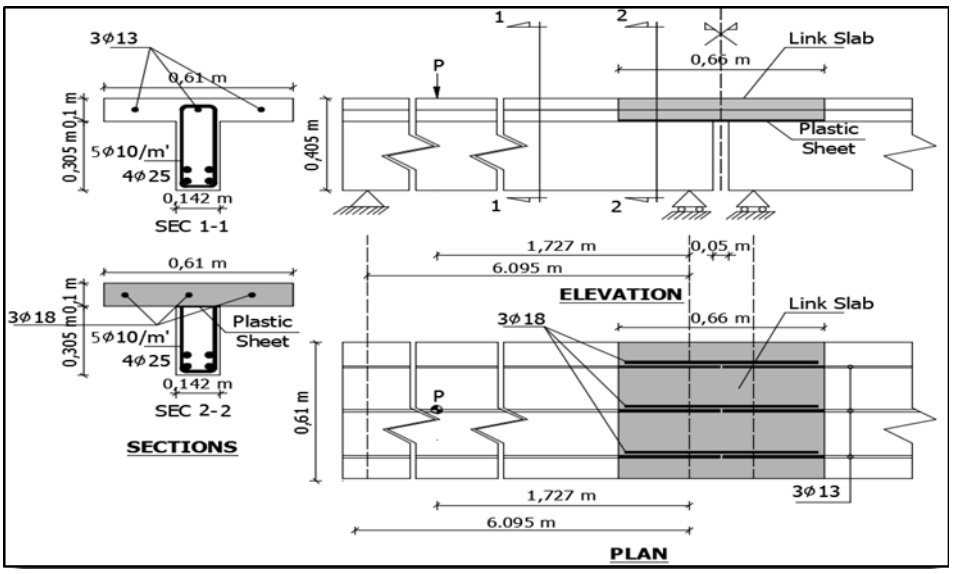

Figure 1. Setup of test bridge with link slab. [10]

In the current research, the former study [13] was modeled using a 3D finite element model, incorporating both geometric and material nonlinearity, in ANSYS software package [25]. The goal of this step is to verify the accuracy and reliability of this model, and to extend its use to cover the parameters of this study.

Four types of elements were used in this verification model, SOLID65 for concrete, SOLID45 for bearing plates, LINK 8 for reinforcement, and contact between link slab and girder was modelled using TARGET 170 and CONTACT 174.

SOLID65, specifically developed by ANSYS for concrete modeling, was utilized to create 3D elements for concrete. This element is able to simulate concrete cracking in tension and concrete crushing in compression. It owns eight nodes and three transitional degrees of freedom in each node. This element is also able to simulate plastic deformation, creep and track stress-strain curve of concrete material. SOLID45, was used for modeling the steel plates at beam supports and under wheel loads. The element is defined with eight nodes having three degrees of freedom at each node, and its behavior was considered linear to effectively allow the distribution of stresses under bearing plates.

LINK 8 was applied to model the reinforcement of the girder, deck and link slab. This element is a nonlinear uniaxial tension-compression element. It has two nodes with three degrees of freedom at each node. This element can rotate, and it has large deflection and large strain capabilities. Contact between link slab and bridge was modeled by contact elements; CONTACT174 and TARGET170. The two elements were utilized to represent contact and sliding between 3D target surfaces using pair- based contact; the target surface is known as TARGET170 and contact surface is known as CONTACT174. This pair configuration allows friction and cohesion between the two surfaces. It also incorporates large displacement capabilities. In this model, the friction and cohesion were eliminated to represent the frictionless surface between link slab and the bridge.

A general overview of the model can be seen in Figure 2. This model is built using 15909 elements and 4780033 nodes. The model was nonlinearly solved under mid- span concentrated loads to failure. And, its support condition was HRRH. The main material properties of the model are presented in Figure. 3 It should be noted that the concrete material, steel and bearing plates were modeled as multilinear isotropic, bilinear isotropic and linear elastic materials, respectively.

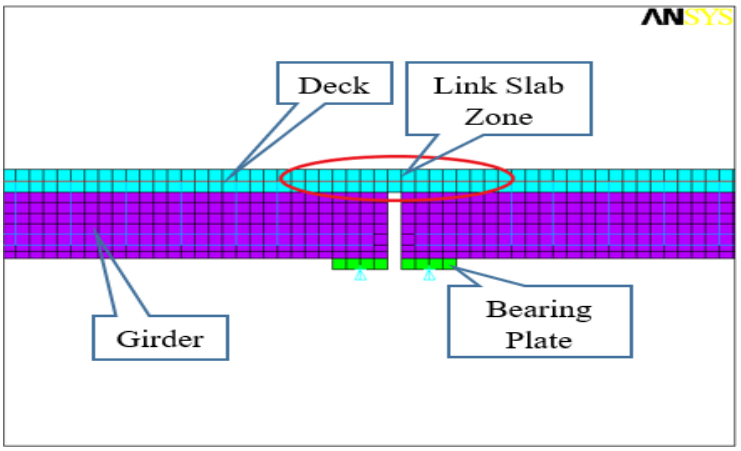

Figure 2. A general overview of the finite element model

Also, the contact zone between girder and link slab was modelled as a frictionless zone. The overlap of deck and link slab reinforcement and the trimmed stirrups in the debonding zone can be also noticed in test setup in Figure 1. The load-deflection results of the model were in a good agreement with experimental results as the difference percentage did not exceed 15%. Also, the tensile stress in the link slab reinforcement was 128.2 MPa at the load of 71 KN with a difference of approximately 5% with the experimental findings. The failure load of the model was about 178 KN with a difference of about 7% with the experimental model.

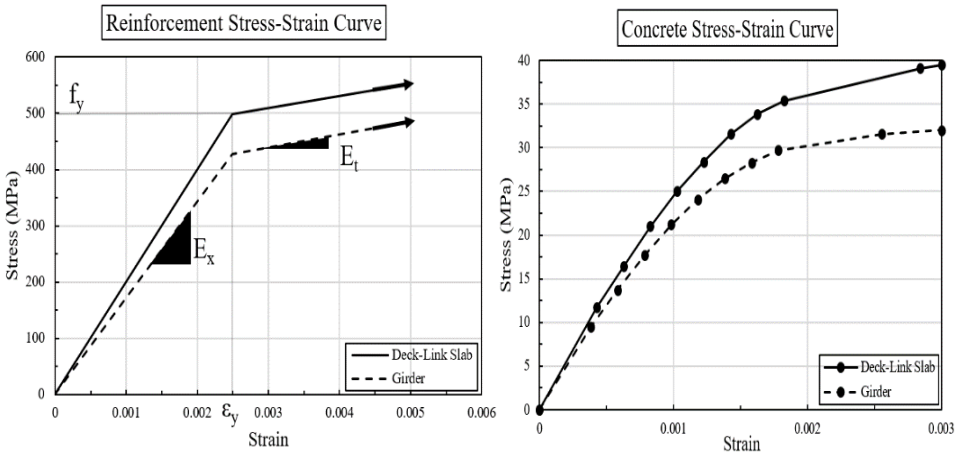

Figure 3. Stress strain curve for both concrete and steel reinforcement.

2.2 Current study bridge and link slab characteristics

An intermediate AASHTO II (PCI) precast pretensioned girder type [24] was considered for modeling, in this study. The bridge was modeled as two simply supported spans of 21.336 m length, each. Figure 4. Shows all the dimensions of the bridge and link slab, and the reinforcement of the bridge at different zones is also depicted. The strands of the girder are 14 strands (grade 270) with a prestressing force of 2740 KN. The strands were extended horizontally along the bottom of the girder.

Regarding the link slab, its width was the same as the bridge width. While, the thickness of the link slab was selected to be 3inch (one-third deck thickness) to reduce its stiffness as much as possible to act as a hinge. The total length of link slab was selected to be (L.S1= 3.2512 m) and (L.S2= 8.5852 m), which represents 7.5% and 20% of the summation of the length of the two girders spans, respectively.

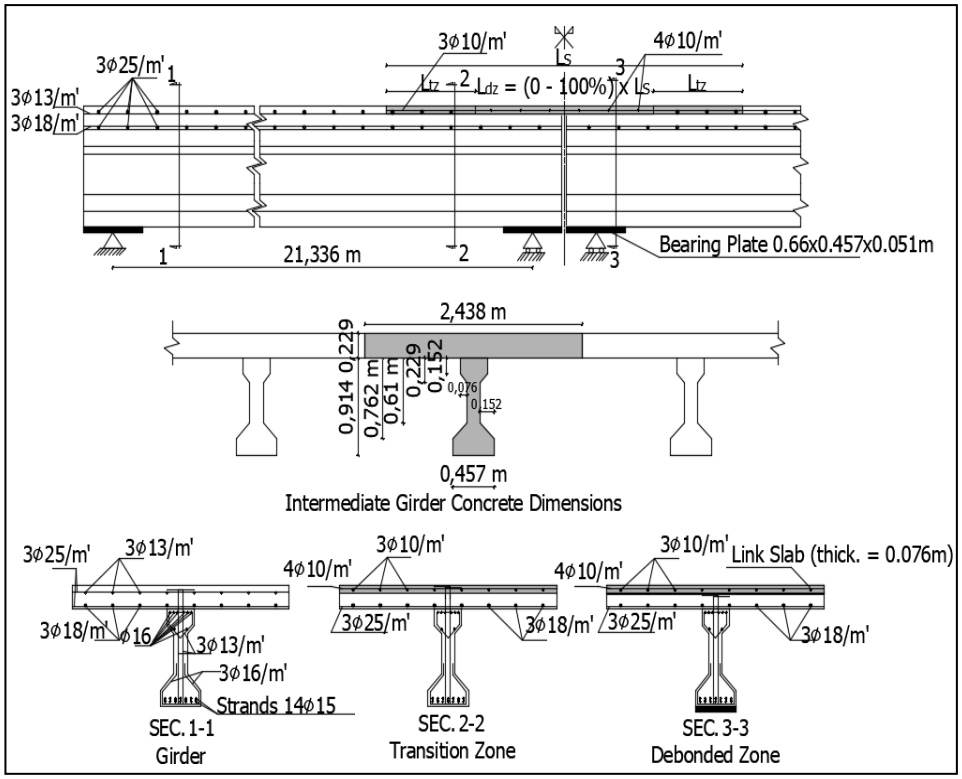

Figure 4. Girder with link slab concrete dimensions and reinforcement.

As previously mentioned, link slab length is divided into two zones; debonding zone (L_{dz}) and transition zone (L_{tz}). The length of the debonding zone (L_{dz}) ranged from 0% to 100% of L_{S1} or L_{S2}. While, the transition zone length (L_{tz}) was the rest of the length of link slab. The reinforcement of link slab consisted of one mesh at the mid depth of the link slab and lab spliced with the top reinforcement of the deck. All the details of the link slab are also illustrated in Figure 4.

The applied loads to the current study bridge were in accordance with AASHTO LRFD Bridge Design Specifications, 6th Edition [24] and the California Amendments to the AASHTO LRFD Bridge Design Specifications (CA) [18]. A standard truck load AASHTO LRFD (HS-93) was applied to the bridge and the bridge was designed due to the gravity, live and impact loads. Figure 5 shows the live load position for the current study bridge (an intermediate girder was considered in this study). While, the material properties utilized for bridge and link slab design are presented in Figure 6.

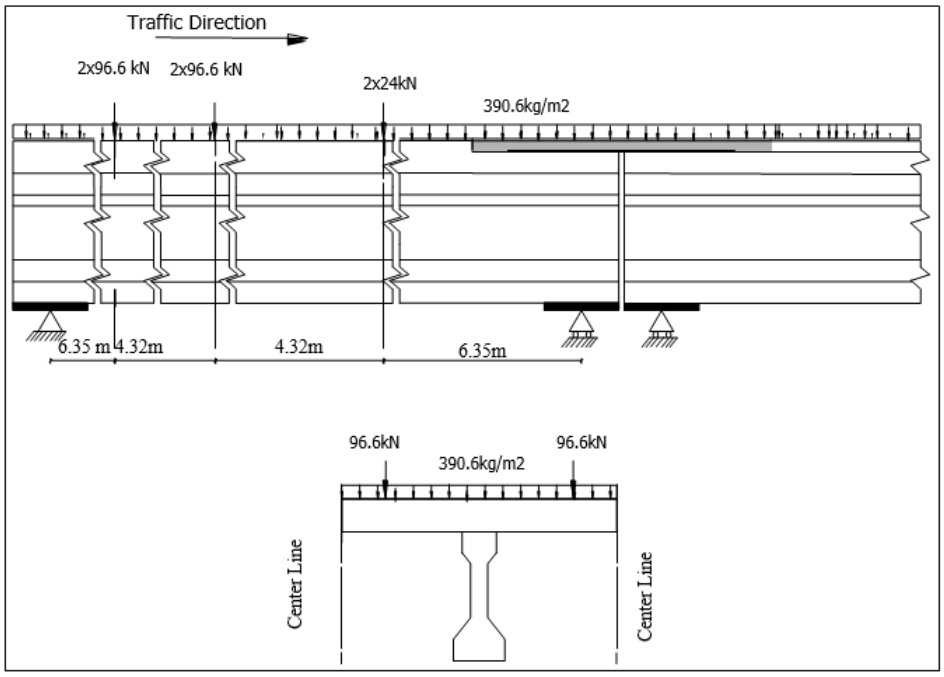

Figure 5. AASHTO (LRFD) load configuration of Highway Bridge.

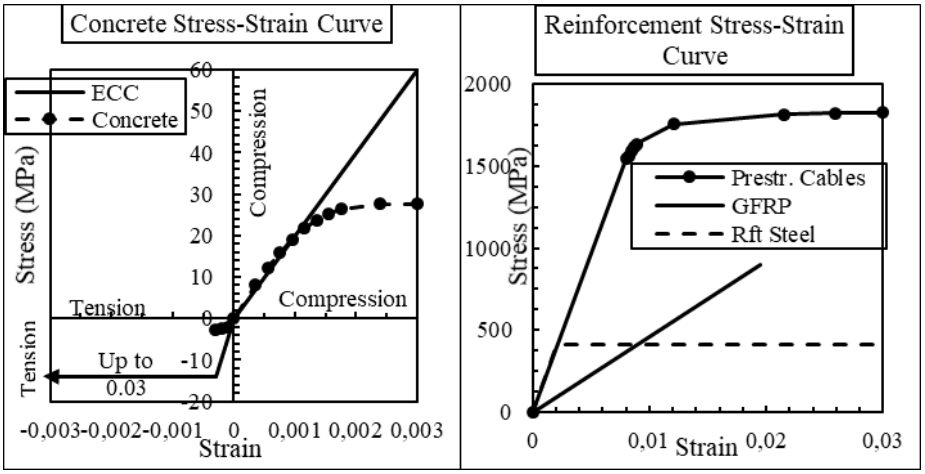

Figure 6. Material properties for current study bridge components.

2.3 Finite Element (F.E) model and analysis of the bridge under study

In order to build the current study model, the same elements utilized in building the verification model were used herein. Additionally, LINK10 element was used to model the prestressing cables. The element has three degrees of freedom

at each node. Stress stiffening and large deflection capabilities are available. Also, the element allows the application of initial stresses to simulate the prestressing of the cable.

The overall geometry of the model is shown in Figure. 7. The live and gravity loads direction is in –Y direction, one interior girder was considered for modelling. Therefore, center line to center link deck geometry was only considered, and, the confinement effect of the rest of the deck was modelled using out of plane supports (in Z direction) at the edges of the deck, as also shown in Figure 7.

A section in the girder and link slab is shown in Figure 7. The contact areas (debonding zone) were considered at the bottom face of the link slab. Also, transition zones were modeled by extending girder stirrups inside the link slab to ensure the composite action between girder and link slab. Moreover, the nodes at bottom face of the link slab at the transition zones were merged with the adjacent bridge nodes.

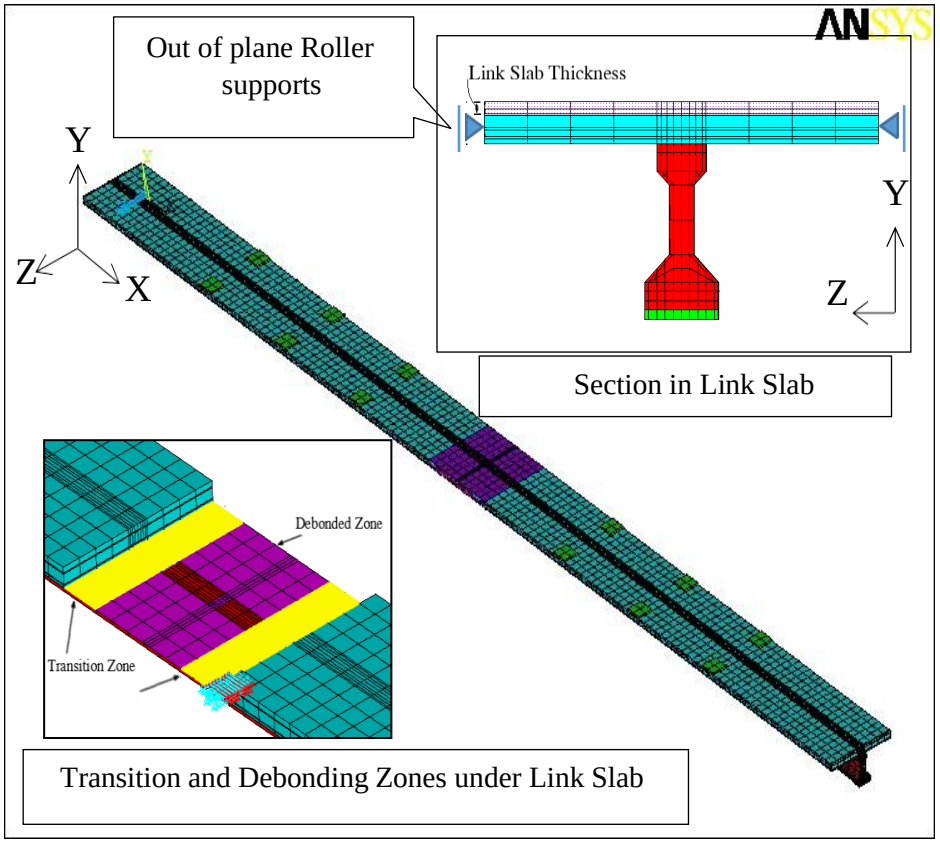

Figure 7. Overview of the bridge's 3D model by ANSYS

The prestressing cables were modeled as straight cables with eccentricity of 0.707m from the neutral axis of the composite section. Also, girder supports were modeled by adding steel plate under the edge of the girder, then, the mid nodes of the plate were constrained either in Y direction (roller support) or in both X and Y directions (hinged support). The same concept of adding steel plates was used to distribute truck wheel loads on the deck.

In order to study the effect of live load on the link slab (to simulate the placement of link slab after the end of bridge construction), the following solution strategy was adopted.

Firstly, the prestressing force and dead load were applied while the link slab elements were excluded from the model by "kill element" simulation option (killing elements in ANSYS is available by assigning a very low stiffness to these elements). After that, in the application of live load on the bridge, the link slab elements were activated again.

2.4 Parametric study

The current study focuses on the following parameters; link slab length, debonding zone length, material type and support conditions. As previously mentioned, the thickness of link slab was selected to be 3inch to reduce its flexural stiffness and its ability to create continuity between bridge girders. The length of the link slab was chosen to be 3.251 m for (L.S1) and 8.585 m for (L.S2).

Various link slab debonding zone lengths (L_{dz}) were considered in this study and ranged from 0% of link slab length in case of full bond with girder to 100% in case of no bond (i.e., no transition zone).

Regarding the material of link slab and its reinforcement, four alternatives were modeled using conventional Concrete (C), Engineered cementitious composites (E), steel Reinforcement (R) and Glass fiber reinforcement polymer bars (G); RC, GC, RE and GE. The applied loadings were limited to gravity and live loads (L.L.) only. Four support conditions were adopted in the current model; RHHR, RHRR, HRRR and HRRH.

3 FINITE ELEMENT MODEL RESULTS AND DISCUSSION

Based on the results of the nonlinear F.E. simulation, the deformed shape and the second order straining actions at the mid-sections of the link slab and the bridge girders were analyzed. Generally, the link slab is subjected to negative moment (tension in the top-most fiber). While, it is affected by compressive forces in the case of HRRH support condition and tensile forces in the rest of support conditions.

This can be explained by the movements of the bridge girders; the girders rotate apart from each other in the case of RHHR and (RHRR or HRRR), generating tensile forces in the mid-section of the link slab. While, they move

toward each other in the HRRH support conditions; as at least one of its supports is roller support, generating compressive forces in the mid-section of the link slab (see Figure 8).

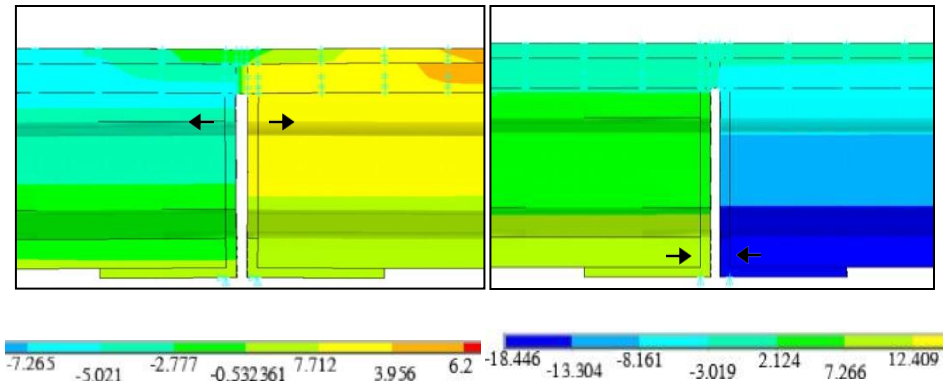

a) RHHR b) HRRH

Figure 8. Contours of the girders' horizontal displacement

Another general finding is that the straining actions in link slab are identical in case of HRRR and RHRR support conditions for each link slab material as can be seen from Figure 9 to Figure 12. Also, the straining actions in link slab are decreasing with the increase of L_{dz}, regardless the material of link slab. This can be related to the minimization of the transferred shear stresses through the interface between bottom face of link slab and the upper face of the adjacent deck.

Regarding RC link slab, the reduction in straining actions (F_X and M_Z) reached about 60% in case of no bond compared to fully bonded link slab, in HRRH support condition. This reduction ratio is nearly the same for both L.S1 and L.S2 link slab lengths. While, this reduction diminishes to about 10% in case of RHHR condition. The case of HRRR and RHRR falls between of the former support conditions with a reduction ratio of about 30% and 50% for both F_X and M_Z, respectively (see Figure 9).

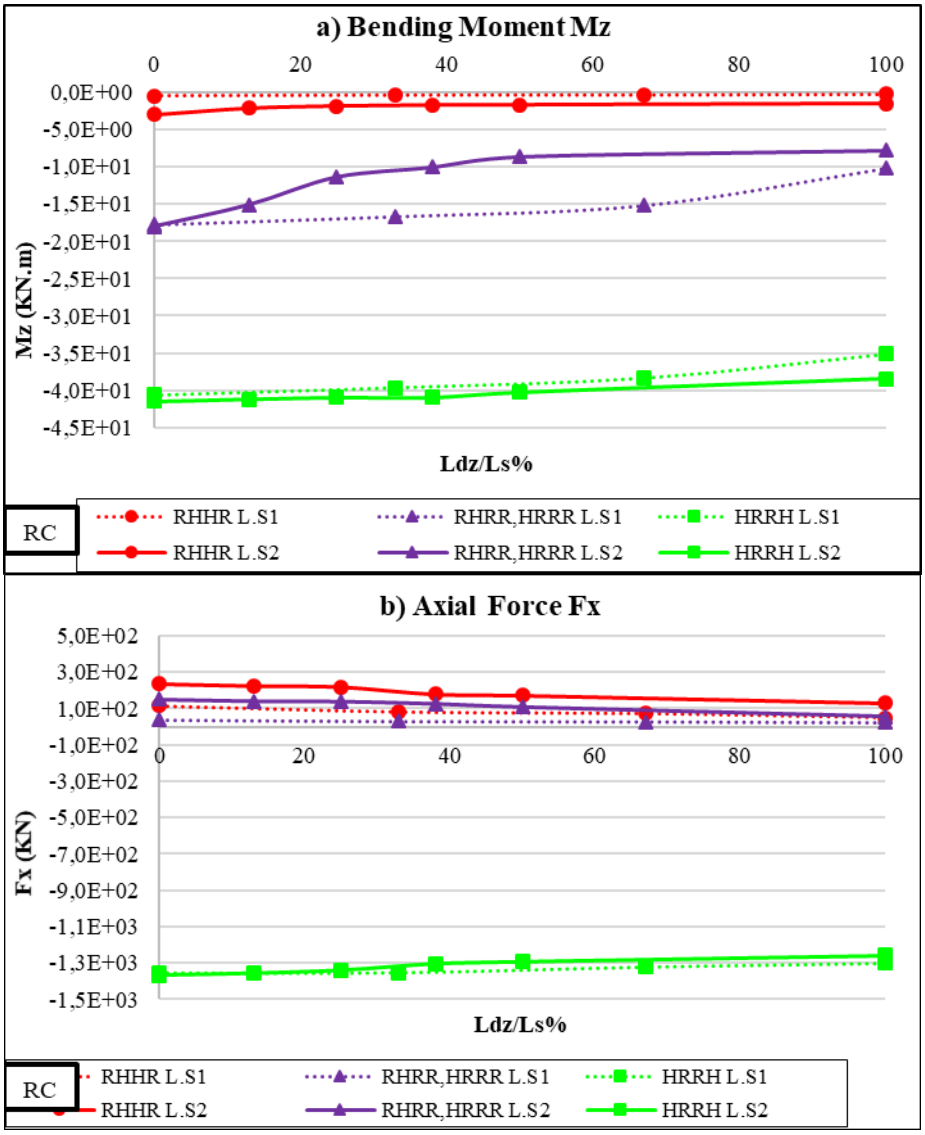

Figure 9. Effect of debonding zone length to link slab length on the straining actions in RC link slab

By comparing GC to RC straining actions, it can be noticed that the generated straining actions in GC link slab are less than RC link slab. This can be attributed to the smaller elastic modulus of G than R material, leading to smaller stresses in G reinforcement and in consequence smaller straining actions. Moreover, the effect of L_{dz} is not clear as much as in RC material as indicated in Figure 10.

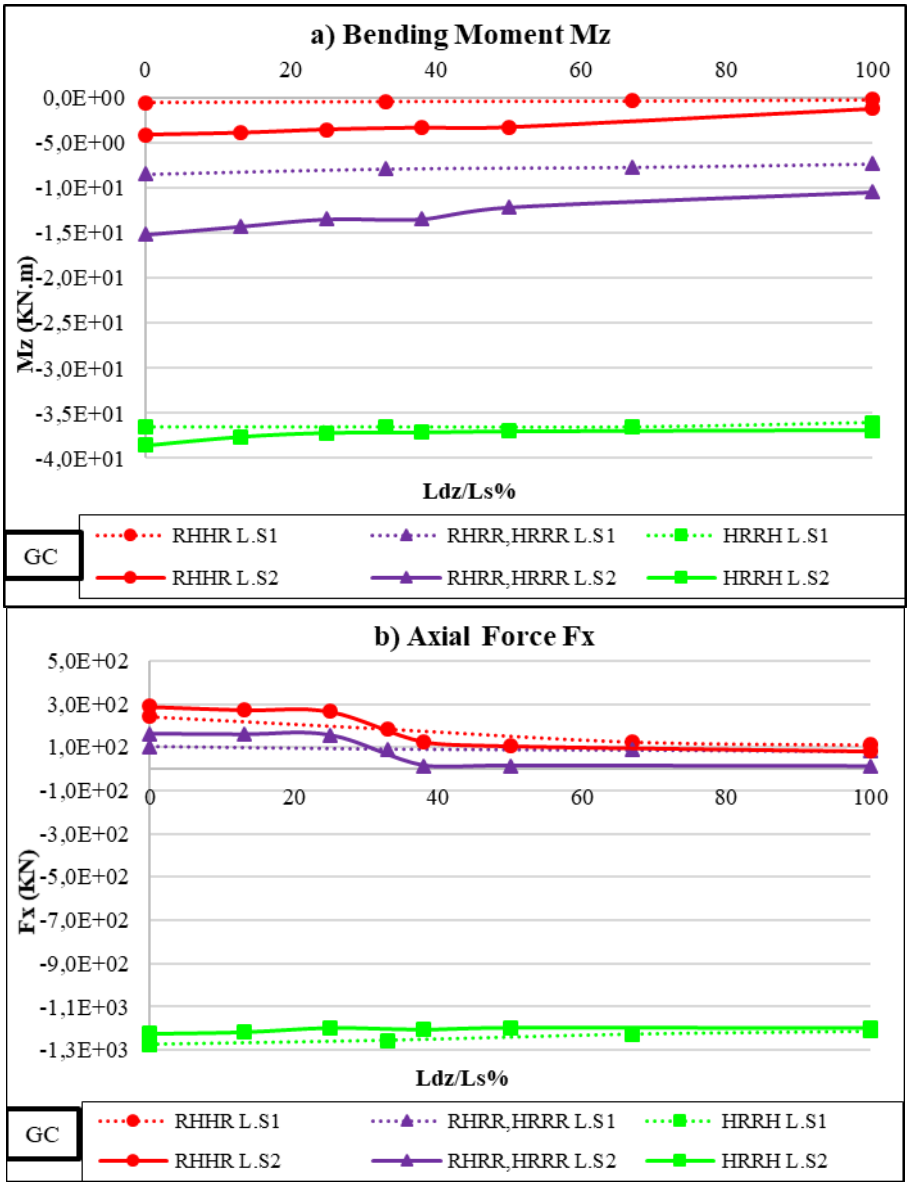

Figure 10. Effect of debonding zone length to link slab length on the straining actions in GC link slab

Regarding ECC materials; RE and GE the straining actions of RE link slab is slightly increased than GE link slab. This can be attributed to the tensile strength of E material and its high tensile strain hardening capabilities. Also, ECC maintains compatible deformation with the steel by continued load transfer through the fibers crossing the micro-cracks. Figures 11, 12 show the straining

actions in the mid-section of link slab. It is obvious that the link slab (either L.S1 or L.S2) is highly stressed in the HRRH support condition. The reduction in the moment for RE is about 15% in case of no bond compared to fully bonded link slab for both L.S1 and L.S2.

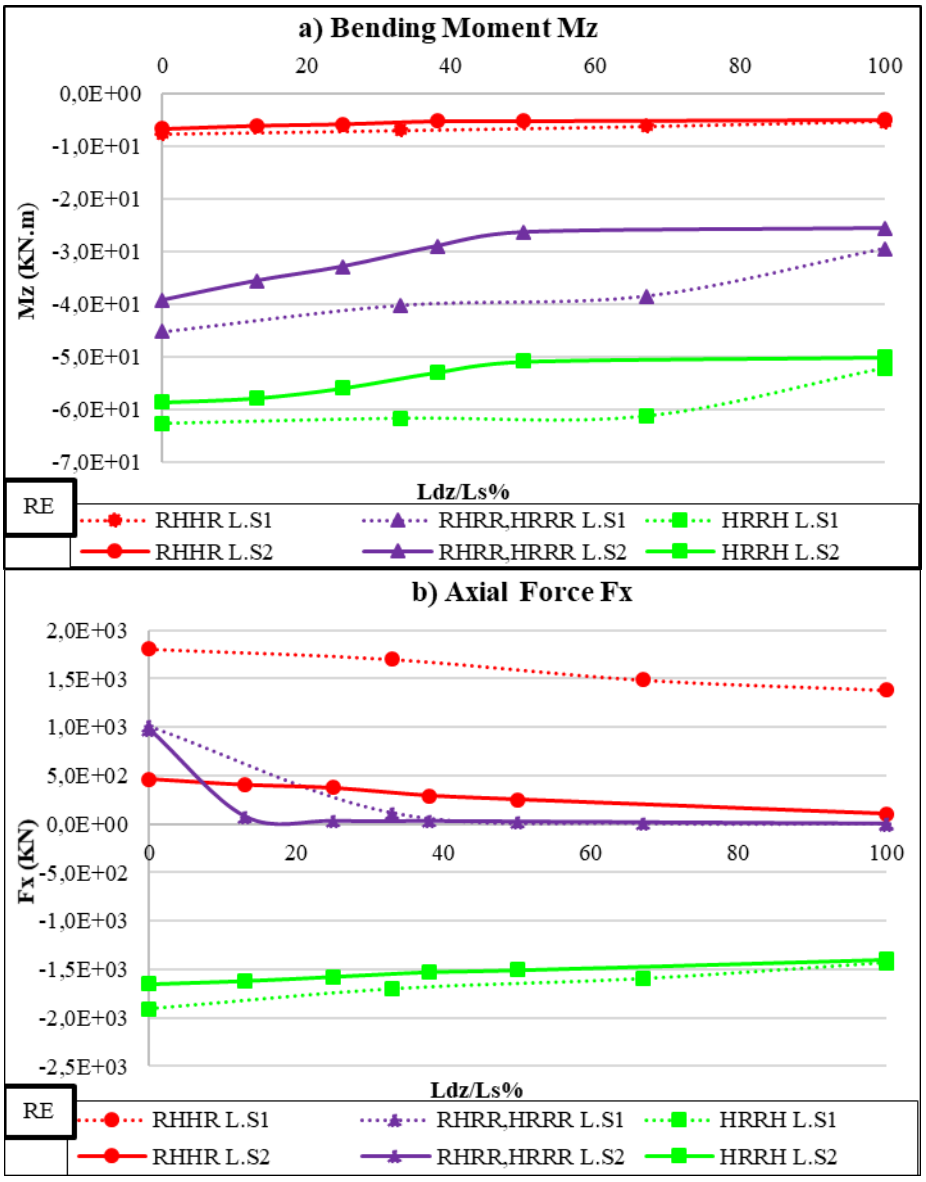

Figure 11. Effect of debonding zone length to link slab length on the straining actions in RE link slab

On the other hand, this reduction ratio in the axial force reaches about 40% and 7% in L.S1 and L.S2, respectively. While, the axial force rapidly decays with the increase of the L_{dz} to about 85% for both L.S1 and L.S2.

By comparing ECC and conventional concrete link slab straining actions, it is obvious that RE and GE link slab is able to drag higher straining actions than conventional concrete link slab. Moreover, the generated tensile force in the L.S1 slab in RHHR condition is about 10 folds that generated in RC and GC link slab. Again, this is due to the tensile strength and high tensile strain hardening of the E material.

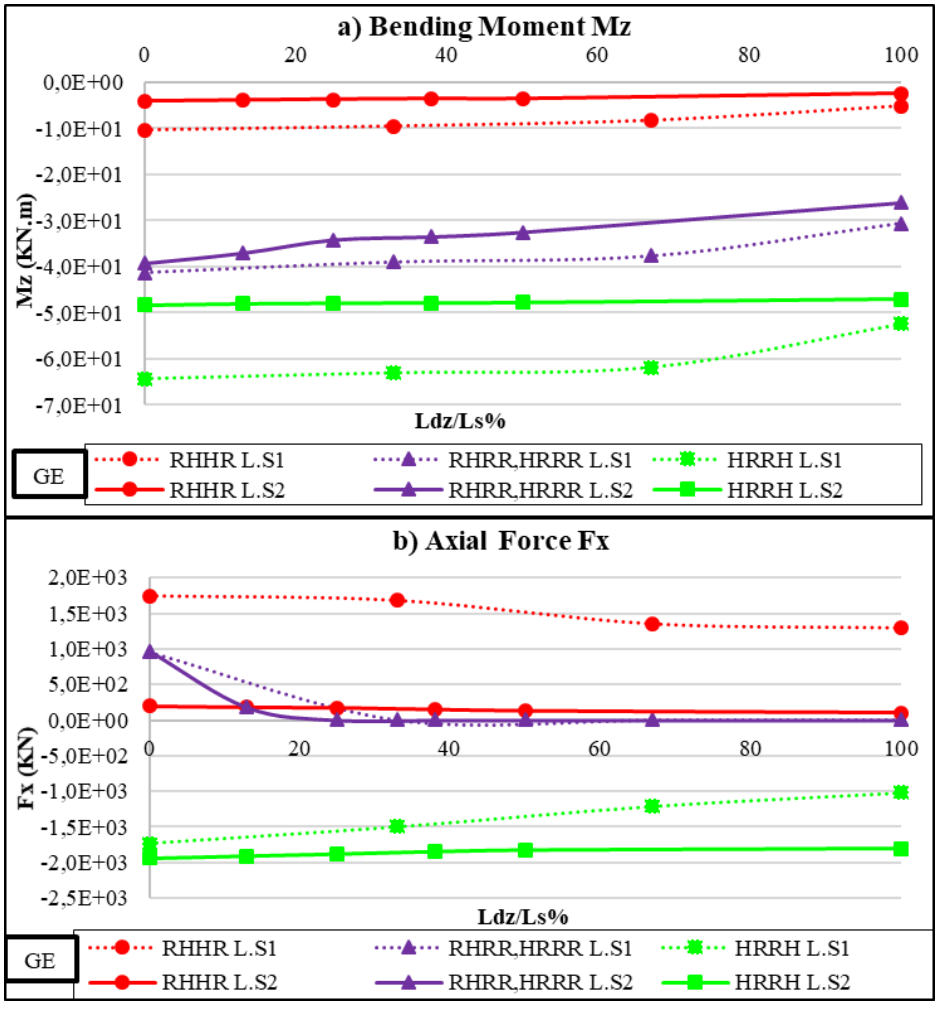

Figure 12. Effect of debonding zone length to link slab length on the straining actions in GE link slab

The results of straining actions are plotted on the interaction diagram (the ultimate capacity of concrete section subjected to combined moment and axial force) of the link slab section. The interaction diagram is constructed based on the stress-strain relations of link slab materials, see Figure 6. The cracked section ultimate stress distribution is shown in Figure 12. It should be noted that the interaction diagram is constructed by varying the compressed zone depth and by computing the resultant ultimate axial force and ultimate moment of the link slab section.

It is worth mentioning that the tensile strength of both conventional concrete and ECC is considered. Moreover, the strain in G bars is checked to not exceed its maximum value in any neutral axis position in the studied section of GC and GE link slab. It can be noticed from Figure 13 that the stresses in the conventional concrete, either compressive or tensile, are considered parabolic, while, the stresses in ECC are linear in compression and constant in tension. The resulted straining action curves are plotted in Figure 14 showing the higher capacity of the RE and GE sections.

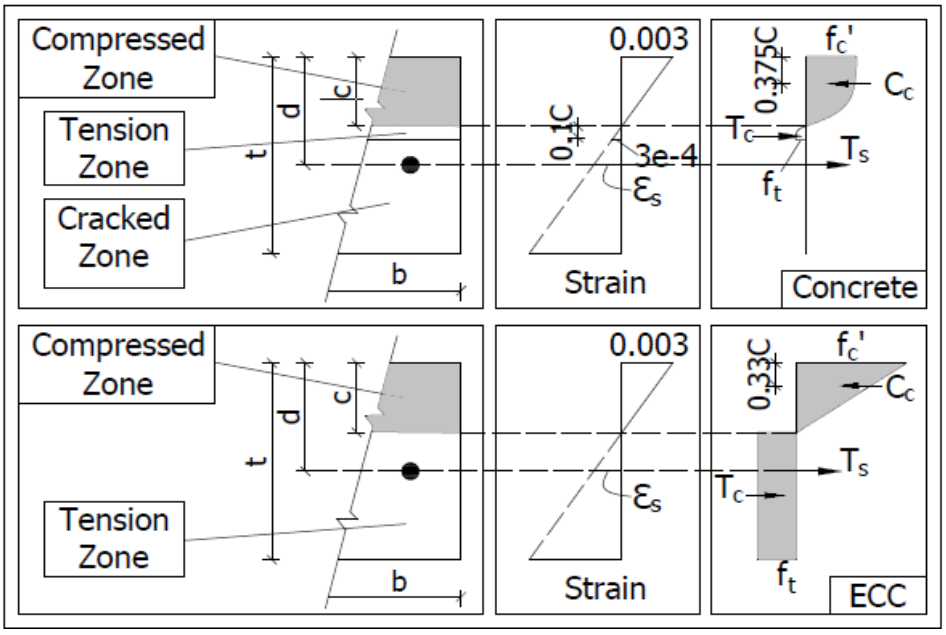

Figure 13. Ultimate stress distribution in link slab section

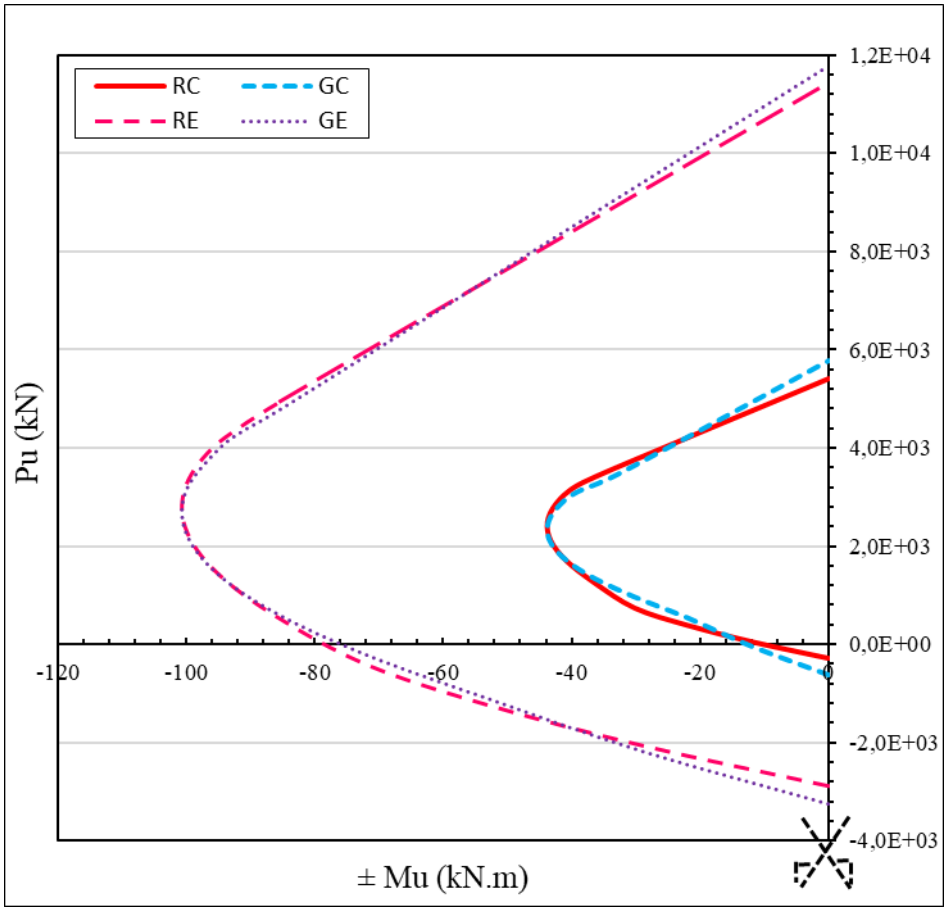

Figure 14. Interaction diagram for link slab various material alternatives

By plotting the resulted straining actions for different link slab materials, it could be noticed that they fall in the tension failure zone, see Figure 15. Also, the increase of L_{dz} leads to safer straining actions in the link slab (i.e., the straining actions shift to the core of the interaction diagram), regardless its material. By inspecting the moment-normal combination for RC link slab, as shown in Figure 15, most of the points are on the verge of failure envelop. Whereas, the increase in Ldz shifts the link slab cross section to safer straining actions combinations. However, factorizing the failure envelopes, for design purposes, for example by 70% or 80%, will certainly lead to unsafe straining actions on these sections. On the other hand, the replacement of steel by G material in GC link slab leads to acceptable straining actions in link slab for all support conditions, except for HRRH.

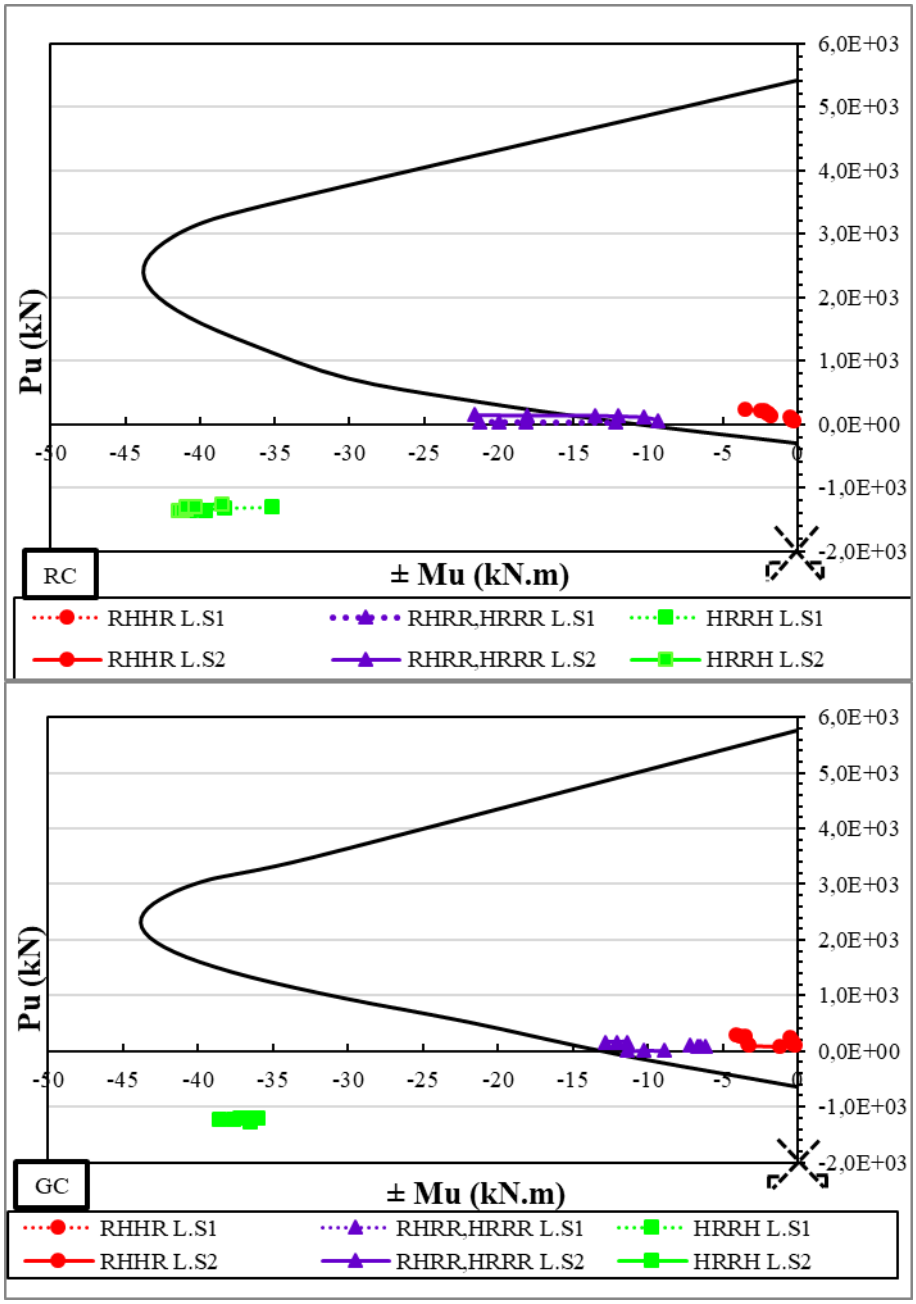

Figure 15. Moment interaction diagram for RC and GC link slab

For RE and GE link slab, all the straining actions fall in safe zones away from failure envelop except HRRH support condition as shown in Figure 16.

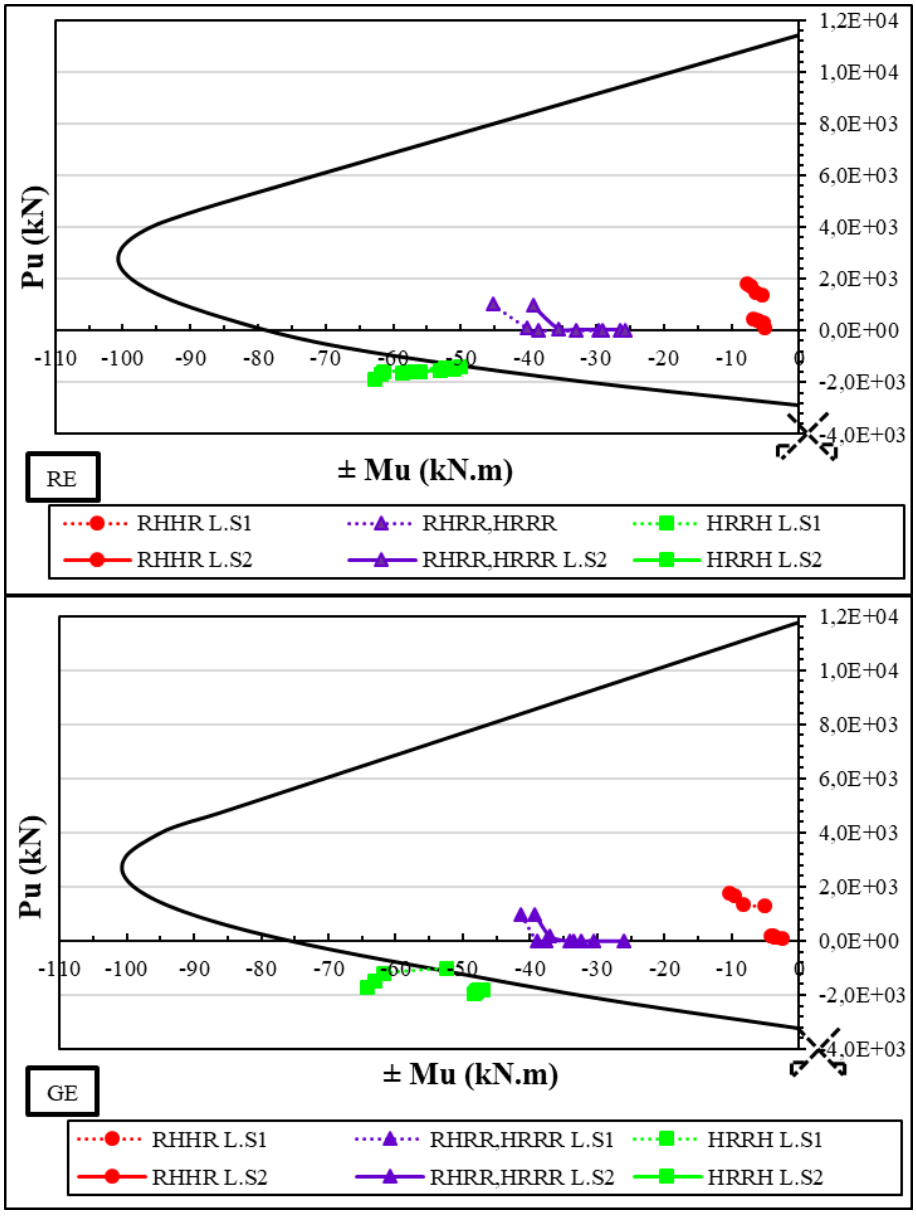

Figure 16. Moment interaction diagram for RE and GE link slab

The serviceability (crack patterns) of link slabs is also studied with the aid of concrete Solid 65 element crack simulation capabilities. It can be noticed from Figure 17. That the conventional concrete suffers from continuous cracks from top to bottom of link slab. This is not acceptable as it creates passages that may lead to corrosion of link slab reinforcement or elements beneath it. It can also be

noticed from Figure 17 that the cracks are widely spread along the link slab in case of RHHR support condition due to the high tensile forces in it. It is worth mentioning that L_{dz} didn't much affect the crack patterns in link slab.

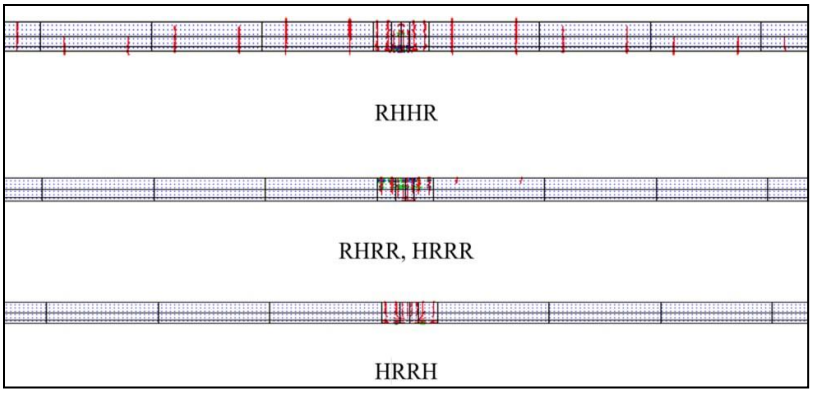

Figure 17. Crack pattern in RC and GC link slab

Figure 18 shows the crack pattern in ECC link slab. It is obvious that the cracks are allocated in the gap zone between girders. Also, these cracks are not covering the whole height of the link slab. Moreover, the cracks in ECC are micro-cracks [12] which means that RE and GE link slabs present safe seal for bridge elements beneath it.

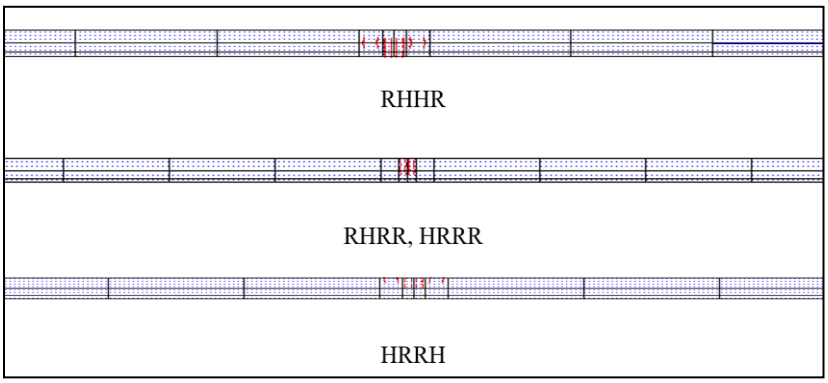

Figure 18. Crack pattern in RE and GE link slab

The M_Z-θ of link slabs are also monitored to obtain the bending stiffness as $K = M_Z/\theta$. The bending stiffness of various L_{dz} were normalized to the bending stiffness fully bonded link slab (i.e., $L_{dz} = 0$) to obtain the bending stiffness ratio, as shown in Figure 19. It was found that the normalized reduction in bending stiffness is not much affected by the reinforcement material. Figure 18 shows this ratio for the RC and RE link slabs. It can be noticed that the

maximum stiffness reduction reaches up to 90% in case of RHHR for fully debonded RC link slab, while, this reduction is limited to about 50% in RHHR, RE link slab.

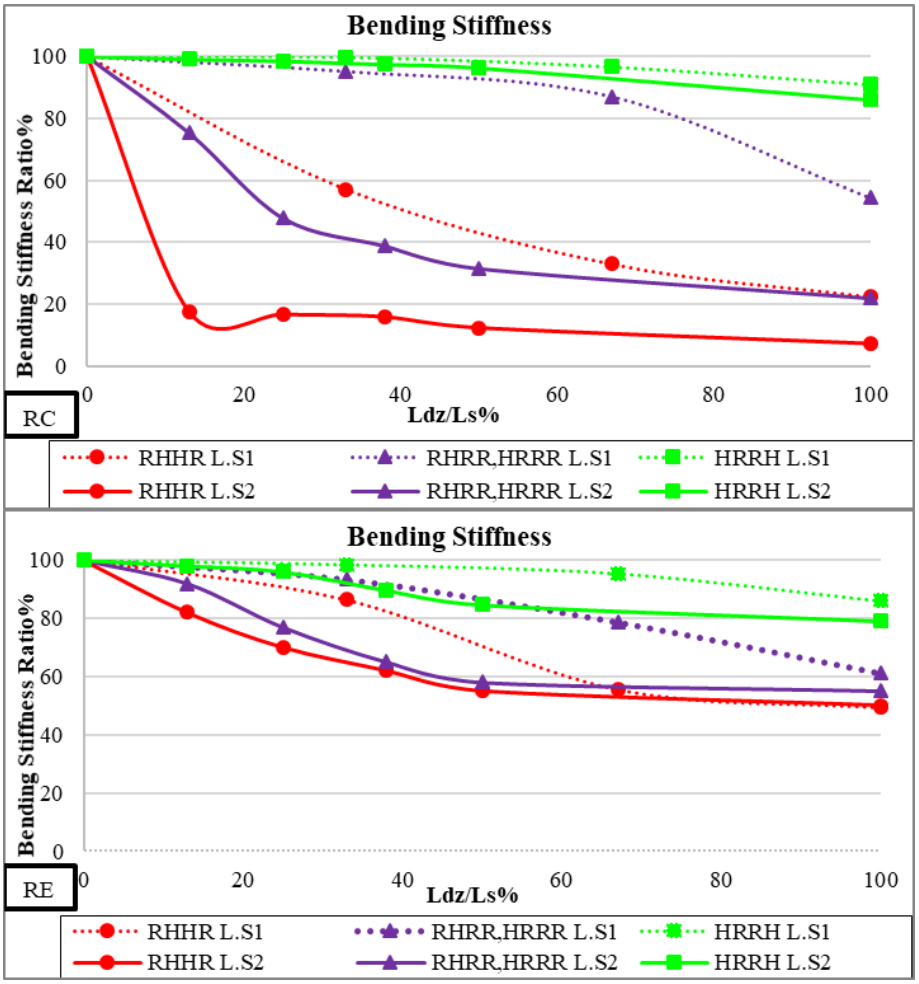

Figure 19. Variation of bending stiffness ratio of RC and RE link slab with debonding length ratio

Regarding GFRP reinforced link slab, bending stiffness ratio, as shown in Figure 20. It can be noticed that the maximum stiffness reduction reaches up to 80% in case of RHHR for fully debonded GC link slab, while, this reduction is limited to about 65% in RHHR, GE link slab.

The effect of link slab on the resulted moment in the girder was also studied. Generally, the effect of L_{dz} is not clear herein, and it can be neglected. The mid-span moment of the girder compared to simply supported girder was studied.

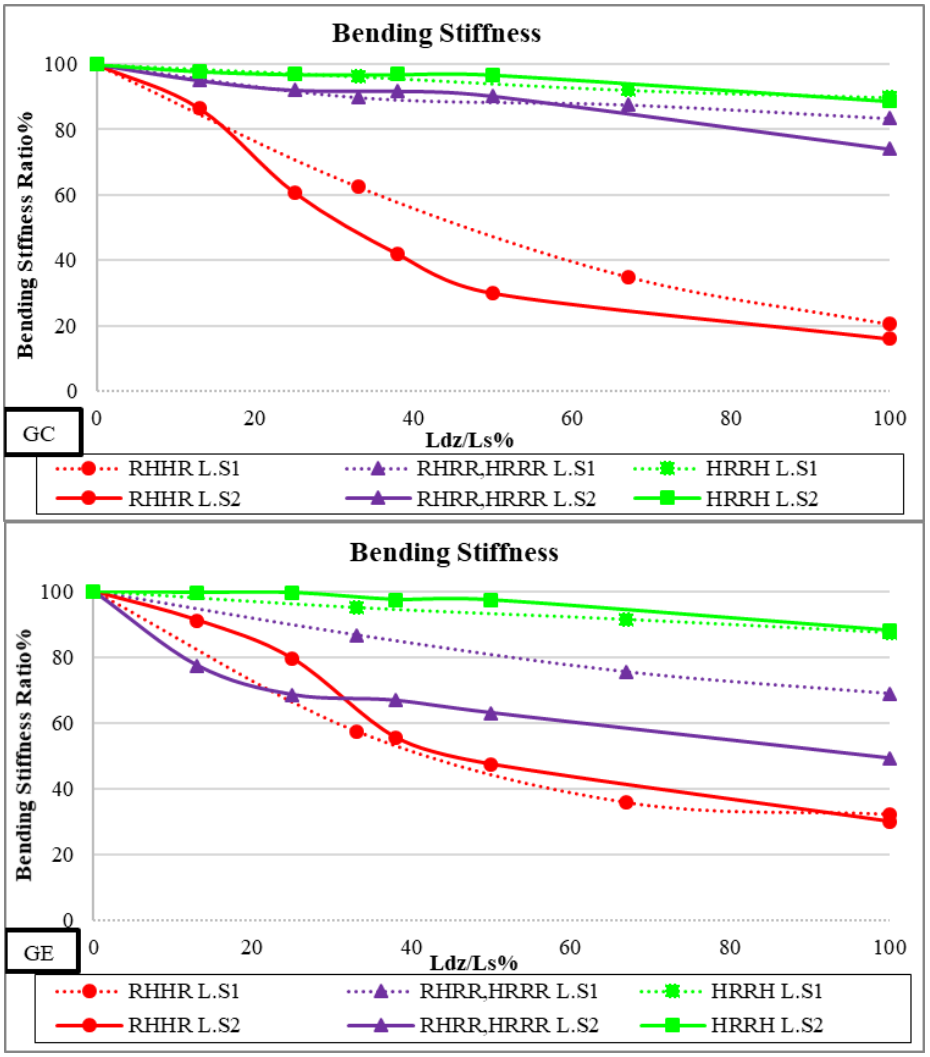

Figure 20. Variation of bending stiffness ratio of GC and GE link slab with debonding length ratio

The presence of the link slab in the RHHR support condition decreases girder moment ratio by about 20% to 30% for various link slab materials and lengths. This can be attributed to the tensile forces generated in the link slab which decrease the end rotation of the girder and its mid-span moment in consequence. On the other hand, the presence of the link slab in the HRRH support condition increases girder moment ratio by about 25% for L.S1, regardless link slab material. This can be explained by the presence of the hinged supports at the far ends of the girders. This means that the girders are forced to move toward each other when loaded. But, the presence of the link slab prevents this movement

leading to the formation of additional stresses in the girder. While, for the case of RHRR and HRRR, the effect of link slab on girder moment ratio is not enormous and can be neglected, as one girder is free to move laterally which prevents the generation of additional stresses in the girder.

4 CONCLUSION

The following points can be concluded from the current study:

1. The mid-section of the link slab is always affected by negative moment, regardless the support condition, the length of the link slab or the length of the debonding zone.
2. The mid-section of the link slab subjected to tensile force in case of RHHR support condition and compression force in the rest of the support conditions.
3. The increase of the debonding zone length leads to decreasing the resulted straining actions in the link slab.
4. The conventional concrete material for link slab is not the optimum choice, as it nearly failed to withstand the resulted straining actions in it.
5. The propagated crack patterns in conventional concrete link slab are continuous from top to bottom of its section and represents a weak point for the durability of the bridge elements beneath it.
6. The reduction in link slab flexural stiffness with debonding zone length may reach severe values in conventional concrete material, while, it is limited to about 40% in ECC material.
7. The presence of link slab led to extra moment in the girders in the case of HRRH support condition, and decreased the moment in case of RHHR condition, while, nearly has no effect in case of RHRR and HRRR.
8. Based on the former point, mounting of link slab on HRRH bridges must be avoided due to its detrimental effect on both the link slab and the bridge girder itself.

Finally, this work recommends a link slab of 3inch thickness made from ECC material with either glass fiber or conventional steel, and the debonding length falls in the range of 80 to 90% of the link slab length for all support conditions, except HRRH.

REFRENCES

[1] Busel, A., Krotau, R., “The design and composition of expansion joints on big-span bridges with intensive heavy-duty traffic”. Transportation Research Procedia, Vol.14, pp. 3953-3962, 2016.

[2] Chang, L. M., and Lee, Y. J., “Evaluation of Performance of Bridge Deck Eexpansion Joints”. Journal of performance of constructed facilities, Vol. 16, No. 3, pp. 3-9, 2002.

[3] Okeil, A.M., and ElSafty, A.” Partial Continuity in Bridge Girders with Jointless Decks”. Practice Periodical on Structural Design and Construction, Vol. 10, No. 4, pp. 229-238, 2005.

[4] Wang, C., Shen, Y., Yun Zou, Y., Zhuang, Y., Tianqi Li, T., “Analysis of Mechanical Characteristics of Steel-Concrete Composite Flat Link Slab on Simply-Supported Beam Bridge”. KSCE Journal of Civil Engineering Vol. 23, No. 8, pp. 3571-3580, 2019.

[5] Canales Jr, Marco Tulio. "Performance Study of Link Slab Continuity in Prestressed Concrete Bridges." 2019.
[6] Oesterle, R. G., Gilkin, J. D., and Larson, S. C. “Design of Precast, Bridge Girder Made Continuous.” Research Rep. No. NCHRP 322, National Research Council, Washington, 1989.
[7] Oskoui, E.A., Taylor, T., Ansari, F., “Method and monitoring approach for distributed detection of damage in multi-span continuous bridges”. Engineering Structures, Vol. 189, pp. 385-395, 2019.
[8] Qian, S., Lepech, M.D., Kim, Y.Y., and Li, V.C. “Introduction of Transition Zone Design for Bridge Deck Link Slabs Using Ductile Concrete”. ACI Structural Journal, Vol. 16, No. 1, pp. 3-96, 2009.
[9] Gastal, F., and Zia, P., "Analysis of Bridge Beams with Jointless Decks." Proceedings of International Association for Bridge and Structural Engineering, pp. 555-560, 1989.
[10] Richardson, Douglas R. "Simplified Design Procedures for the Removal of Expansion Joints from Bridges Using Partially Debonded, Continuous Decks." PhD diss., North Carolina State University, 1989.
[11] El-Safty, A.K. "Analysis of jointless bridge decks with partially debonded simple span beams." PhD Dessertation, North Carolina State Univ., Raleigh, NC 1994.
[12] Loveall, Clellon L. "Jointless bridge decks" Civil Engineering Vol. 55, No. 11, pp. 64-67, 1985.
[13] Caner, A., and Zia, P. “Behavior and Design of Link Slabs for Jointless Bridge Decks.” Math. Intell, Vol. 43, No. 3, pp. 68-80, 1998.
[14] El-Safty, Adel, and Ayman M. Okeil. "Extending the service life of bridges using continuous decks." PCI journal, Vol. 53, No. 6, pp. 96-11, 2008.
[15] Ulku, Evren, Upul Attanayake, and Haluk Aktan. "Jointless bridge deck with link slabs: Design for durability." Transportation research record, 2131, No. 1, pp. 68-78, 2009.
[16] Okeil, Ayman M. "Evaluation of continuity detail for precast prestressed girders: tech summary.” Vol. 101, No. 6, pp. 11- 477, 2011.
[17] Okeil, Ayman M., Tanvir Hossain, and C. S. Cai. "Field monitoring of positive moment continuity detail in a skewed prestressed concrete bulb-tee girder bridge." PCI journal, Vol. 58, No. 2, 2013.
[18] Kim, Y.Y., Fischer, G., and Li, V.C. “Performance of Bridge Deck Link Slabs Designed with Ductile Engineered Cementitious Composite”. Structural Journal, Vol. 101, No. 6, pp. 792-801, 2004.
[19] Zheng, Y., Zhang, L.F., Xia, L.P., “Investigation of the behaviour of flexible and ductile ECC link slab reinforced with FRP”. Construction and Building Materials, Vol. 166, pp. 694–711, 2018.
[20] Li, V.C., Fischer, G., Kim, Y., Lepech, M.D., Qian, S., Weimann, M., and Wang, S. “Durable Link Slabs for Jointless Bridge Decks Based on Strain- Hardening Cementitious Composites” (No. Research Report RC-1438), U.S.A, 2003.
[21] Kanda T., Lin Z., Li V.C. “Application of Pseudo Strain-Hardening Cementitious Composites to Shear Resistant Structural Elements.” Aedificatio Publishers; Freiburg, Germany, pp. 1477-1490, 1998.
[22] Zhang, J., and Li, V.C. “Monotonic and Fatigue Performance in Bending of Fiber-Reinforced Engineered Cementitious Composite in Overlay System”. Cement and Concrete Research, Vol. 32, No. 3, pp. 415-423, 2002.
[23] Sahmaran, M. Lachemi, M. Hossain K. M.A. Ranade, R. and Li, V.C. “Internal Curing of ECC’s for Prevention of Early Age Autogenous Shrinkage Cracking”. Cement and Concrete Research, Vol. 39, No. 10, pp. 893-901, 2010.
[24] AASHTO. “AASHTO LRFD Bridge Design Specifications” 6th Edition, Washington, 2012.
[25] ANSYS 12 user’s manual, Ansys Inc.
[26] Caltrans., California Amendments to AASHTO LRFD Bridge Design Specifications – 6th Edition, California Department of Transportation, Sacramento, California.